Bull. Chem. Soc. Ethiop. **2025**, 39(9), 1779-1793.
DOI: https://dx.doi.org/10.4314/bcse.v39i9.10

ISSN 1011-3924
Printed in Ethiopia
Online ISSN 1726-801X

NATURAL OILS AS EMULSIFYING AGENT IN THE ECO-FRIENDLY PREPARATION OF NANO ZnO AND THEIR CATALYTIC EVALUATION IN THE SYNTHESIS OF 1,8-DIOXO-OCTAHYDROXANTHENE DERIVATIVES WITH ANTI-INFLAMMATORY ACTIVITY: IN VITRO, DOCKING VALIDATION, AND DFT CALCULATIONS

Heba M. Metwally[1], Yasmen Osama[1], Ehab Abdel-Latif[1], Abdulrahman A. Almehizia[2], Ahmed M. Naglah[2*], Hazem A. Ghabbour[3,4] and Tamer K. Khatab[5*]

[1]Department of Chemistry, Faculty of Science, Mansoura University, Mansoura 35516, Egypt
[2]Drug Exploration & Development Chair (DEDC), Department of Pharmaceutical Chemistry, College of Pharmacy, King Saud University, P.O. Box 2457, Riyadh 11451, Saudi Arabia
[3]School of Health and Biomedical Sciences, RMIT University, Melbourne 3083, Australia
[4]Department of Medicinal Chemistry, Faculty of Pharmacy, Mansoura University, Mansoura 35516, Egypt
[5]Organometallic and Organometalloid Chemistry Department, National Research Centre, Dokki, 12622, Giza, Egypt

(Received February 3, 2025; Revised April 11, 2025; Accepted May 12, 2025)

ABSTRACT. In the present work, bio-based ZnO nanoparticles were prepared using environmentally friendly methods. FTIR, XRD, and TEM illustrated the chemical structure of the prepared NPs. The nano ZnO was used as a catalyst to prepare xanthene compounds in one-step reactions by mixing two moles of dimedone and aromatic aldehyde under solvent-free conditions at 60-70 ºC. After the specified time for the completion of the reaction, the products were separated and their structural forms were confirmed using IR, NMR and MS. The prepared xanthene derivative compounds undergo biological evaluation as COX1, COX2 and 5-LOX inhibitors. For example, it was noticed that ligand **6** inhibited the activities of COX-1 and COX-2 by 77.28±0.18 and 79.53±0.18 %, respectively. Compared to the standard indomethacin (a nonsteroidal anti-inflammatory drug), which inhibited the activities of COX-1 and COX-2 by 85.20±0.01 and 87.35±0.01 %, respectively. Also, ligand **6** presented the lowest IC_{50} values (5.96±0.04, 5.27±0.02 and 7.77±0.03 mg/mL, respectively) against COX-1, COX-2 and 5-LOX enzymes. Based on the data obtained from DFT (density functional theory) calculations, docking studies, and biological evaluations as inhibitors of COX-1, COX-2, and 5-LOX enzymes, it was determined that four derivatives (**4**, **6**, **7**, and **10**) have potential for in vivo anti-inflammatory testing.

KEY WORDS: Zinc oxide, Xanthene, Nanoparticles, Anti-inflammatory, DFT

INTRODUCTION

A novel approach to catalysis and "green" chemical synthesis, nano catalysis was introduced in the 21st century [1]. These catalysts are attractive alternatives to conventional ones because of their excellent selectivity, high catalytic activity, large surface-to-volume ratio, and often greater stability. They can significantly affect organic synthesis by functioning as semi-heterogeneous catalysts [2, 3]. Zinc oxide has recently become a fascinating metal oxide material due to its distinct physical and chemical characteristics like excellent chemical and mechanical stability, strong catalytic activity, coefficient of electrochemical coupling, wide radiation absorption capabilities, and non-toxic characteristics [4]. It also exhibits distinctive optical, electrical, photochemical, or catalytic capabilities, which is why zinc oxide nanoparticles ZnO-NPs are used in various biological and commercial applications. They protect wood and textiles from ultraviolet

*Corresponding authors. E-mail: anaglah@ksu.edu.sa ; tamer_khatab@hotmail.com

degradation [5]. Additionally, ZnO-NPs possess the ability to inhibit harmful bacteria and are produced through environmental methods [6]. ZnO-NPs serve as a cross-linking agent and treatment activator within the rubber industry, facilitating an accelerated vulcanization process for rubbers utilized in the production of balloons, tires, rubber products, as well as industrial and medical gloves [7]. Due to their diverse applications, the scientific community highly values the production of ZnO-NPs. Several methods have been developed to synthesize ZnO-NPs, categorizing them as physical, chemical, or green approaches. The chemical process includes solvothermal methods, sol-gel, chemical bath deposition, hydrothermal, wet techniques, microemulsion, spray pyrolysis, and precipitation [8]. The physical techniques are magnetron sputtering, pulsed laser deposition, electron beam evaporation, and electrodeposition [9]. It is noted that most methods require expensive chemicals and also have notes on their degree of toxicity. Hence, the green pathway by using a capping agent for stabilizing nanoparticles will be presented in this research.

Multicomponent reactions MCRs continue to be a valuable option in organic synthesis serving a wide range of applications including medicinal chemistry, drug discovery, green chemistry, polymerization, and related fields [10-12]. MCRs exhibit a high degree of convergence and demonstrate favorable atom, step, and pot economy. However, due to the limited number of MCRs documented in the literature, employing post-condensation modifications represents an effective approach to broaden the range of MCRs and develop novel and more complex molecular structures [13-16].

Xanthene's heterocycles and their derivatives are an important class of natural products, that exhibit a wide range of biological activities including anti-inflammatory [17], anti-malarial, anti-depressant agents [18], photosensitizers in photodynamic therapy [19], anti-bacterial [20], and anti-viral [21]. It can be used in industrial sectors as fluorescent material [22], dyes [23], and laser technology [24]. Several techniques have been reported for the synthesis of xanthenes and their derivatives, such as the cyclic acylation process of carbamates [25], the capture of benzynes by phenols [26], cyclodehydrations [27], intra-molecular phenyl–carbonyl coupling reactions [28], and the reaction of aryloxy magnesium halides with triethyl orthoformate [29]. The synthesis of xanthene can be facilitated by a variety of catalysts, including silica sulfuric acid [30], triethyl benzyl ammonium chloride [31], amberlyst-15 [32], and $NaHSO_4$-SiO_2 [33]. The drawbacks of these methods associated with these techniques include the reliance on costly and hazardous reagents/ organic solvents /catalysts, extended reaction times, creation of toxic by-products, and low yields. To overcome the mentioned limitations along with the increasing environmental concerns, there is a significant potential for the development of enhanced, practical, and eco-friendly methods for the synthesis of xanthenes and their derivatives.

EXPERIMENTAL

The stabilizer compounds, propylene glycol, aloe vera, jojoba oil, caprylic/capric triglyceride, and flaxseed gel labeled as "natural", were bought from Sigma Aldrich. Purchased from a nearby marketing company called "PioChem" were $ZnCl_2$, NaOH, and MeOH.

Green synthesis of ZnO-NPs

Initially, 10 g of a natural substance with stabilizing or emulsifying properties were combined with 10 mL of MeOH and mixed for 15 min. Subsequently, 3 g, equivalent to 0.02 mol, of $ZnCl_2$ were introduced. With vigorous stirring, a burette was used to slowly add an alkaline solution (40 g of NaOH in 100 mL water) to the mixture of $ZnCl_2$ and natural compound. Following the addition, the reaction was left to stir at room temperature for the entire night. A white solid was formed, filtered, and then rinsed with distilled water to purify it. Following this, the solid was

subjected to two different drying steps: one at 100 °C for 18 hours and another at 400 °C for 4 hours.

Characterization of ZnO-NPs

Zinc oxide nanoparticles (ZnO-NPs) were analyzed for morphology using transmission electron microscopy (TEM), X-ray diffraction (XRD), and Fourier transform infrared spectroscopy (FTIR).

Chemicals and instrumental analysis

Gallenkamp, a German device, was used to measure the melting points. The infrared spectra (KBr) were recorded using Thermo Fisher Nicolet iS10 in the USA. The ^{1}H NMR and ^{13}C NMR spectra were recorded using two different spectrometers: Bruker Avance III: ^{1}H NMR: 400 MHz, ^{13}C NMR: 100 MHz and Jeol: ^{1}H NMR: 500 MHz, ^{13}C NMR: 125 MHz. The NMR measurements were performed with solvents DMSO-d_6 and chloroform. The Kratos MS device he used captured mass spectra in EI mode with an ionization voltage of 70 eV. Elemental analyses were performed using an instrument analyzer from the EuroVector (EA3000 series). TLC was employed for monitoring the reaction mixture, while silica gel-coated plates were illuminated with UV light for visualization purposes.

Organic reaction procedure

Aldehydes (10 mmol), dimedone (20 mmol), and 0.2 g, 25 mol percent of ZnO-NPs were mixed and keep to stirring at 60-70 °C. The progression of the reaction was monitored with thin layer chromatography (TLC) until the initial components were no longer visible. The organic product was extracted using 20 mL of chloroform, followed by the purification of the products through recrystallization in ethanol as solvent.

*4-(3,3,6,6-Tetramethyl-1,8-dioxo-2,3,4,5,6,7,8,9-octahydro-1H-xanthen-9-yl)phenyl benzoate (**7**).* Yield = 95%, m.p. = 185-190 °C, pale orange powder. IR (υ/cm^{-1}):1733 (-O-C=O), 1575-1595 (enone + Ar. -C=C-). ^{1}H NMR (δ/ppm); ($CHCl_3$): 12.10 (enolic O-H), 7.61-7.09 (m, 9H, ArH), 4.67 (s, 1H, –CH), 2.37 (s, 4H, 2×–CH_2), 2.33 (s, 4H, 2×–CH_2), 1.08 (s, 12H, 4×–CH_3). ^{13}C NMR (δ/ppm); ($CHCl_3$): 190.92-189.25 (2 C=O), 165.08 (ester O-C=O), 148.80 37 (2C, =C-O-C=), 133.45-121.26 (13 Ar. C), 115.43 (=C-C=O), 46.65 (methylene 2x CH_2-C=O), 32.25 (1 C), 31.36 (methylene 2x CH_2)), 29.55 (quaternary 2 C-CH_3), 27.36 (4 CH_3). MS (EI) *m/z* = 470[M]$^{+}$. Anal. calcd. for $C_{30}H_{30}O_5$ (470.21): C, 76.57; H, 6.43; O, 17.00%. Found: C, 76.43; H, 4.33; O, 16.92%.

*4-(3,3,6,6-Tetramethyl-1,8-dioxo-2,3,4,5,6,7,8,9-octahydro-1H-xanthen-9-yl)phenyl 4-methylbenzoate (**8**).* Yield = 93%, m.p. = 165-180 °C, Pale yellow powder. IR (υ/cm^{-1}): 1734 (-O-C=O), 1570-1590 (enone + Ar. -C=C-). ^{1}H NMR (δ/ppm); (DMSO): 7.99-6.99 (m, 8H, Ar.H), 4.61 (s, 1H, –CH), 2.40 (s, 3H, –CH_3), 2.23 (s, 4H, 2×CH_2), 2.22 (s, 4H, 2×–CH_2), 1.00 (s, 12H, 4×CH_3). ^{13}C NMR (δ/ppm); (DMSO): 187.38 (C=O), 164.68 (ester O-C=O), 147.69 (HO-C=C-H), 144.37 (2C, =C-O-C=), 129.78-114.44 (14 Ar.C+ olefinic H-C=C-OH)), 47.54 (methylene, 2x CH_2-C=O), 31.24 (methylene, 2x CH_2-C=C)), 30.98-30.16 (quaternary 2x C-CH_3 + 1C), 28.09 (4 CH_3), 21.27 (Ar-CH_3). MS (EI) *m/z* = 484 [M]$^{+}$. Anal. calcd. for $C_{31}H_{32}O_5$ (484.22): C, 76.84; H, 6.66; O, 16.51%. Found: C, 76.73; H, 6.55; O, 16.41%.

*4-(3,3,6,6-Tetramethyl-1,8-dioxo-2,3,4,5,6,7,8,9-octahydro-1H-xanthen-9-yl)phenyl 4-methylbenzenesulfonate (**9**).* Yield = 98%, m.p. = 160-170 °C, pale yellow powder. IR (υ/cm^{-1}):

1570-1600 (enone + Ar. -C=C-). ^{1}H NMR (δ/ppm); (DMSO): 7.69 - 6.79 (m, 8H, ArH), 4.33 (s, 1H, –CH), 2.39 (s, 3H, –CH_3), 2.26 (s, 4H, 2×–CH_2), 2.25 (s, 4H, 2×–CH_2), 0.98 (s, 12H, 4×–CH_3). ^{13}C NMR (δ/ppm); (DMSO): 187.14 (2 C=O), 146.46-145.85 (2C, =C-O-C=), 130.19 - 114.15 (14 Ar.C), 46.79 (methylene, 2x CH_2-C=O), 32.56-31.25 (methylene, 2x CH_2-C=C + 1C), 30.35 - 29.08 (quaternary 2x C-CH_3), 27.84 (4 CH_3), 21.17 (Ar-CH_3). MS (EI) *m/z* = 520 $[M]^+$. Anal. calcd. for $C_{30}H_{32}O_6S$ (520.19): C, 69.21; H, 6.20; O, 18.44; S, 6.16%. Found: C, 69.11; H, 6.11; O, 18.34; S, 6.09%.

*9-(3-(4-Chlorophenyl)-1-phenyl-1H-pyrazol-4-yl)-3,3,6,6-tetramethyl-3,4,5,6,7,9-hexahydro-1H-xanthene-1,8(2H)-dione (**10**).* Yield = 98%, m.p. =185-200 °C, Yellow powder. IR (υ/cm^{-1}): 1560 - 1585 (amide + enone + Ar. -C=C-). ^{1}H NMR (δ/ppm); (DMSO): 7.77 - 7.26 (m, 10H, ArH), 4.55 (s, 1H, –CH), 2.05 (s, 4H, 2×–CH_2), 2.03 (s, 4H, 2×–CH_2), 0.97 (s, 12H, 4×–CH_3). ^{13}C NMR (δ/ppm); (DMSO): 186.34 (2 C=O), 149.09 (2C, =C-O-C=), 139.88 (C=N), 130.51 - 114.43 (16 Ar.C), 46.85 (Methylene, 2x CH_2-C=C), 32.12 (1C), 30.88 (Methylene, 2x CH_2-C=C), 27.68 (quaternary 2x C-CH_3), 22.90 (4 CH_3). MS (EI) m/z = 526/528 $[M^+/M^+{+}2]$. Anal. calcd. for $C_{32}H_{31}ClN_2O_3$ (526.20): C, 72.92; H, 5.93; N, 5.32; Cl, 6.73; O, 9.11%. Found: C, 72.81; H, 5.82; N, 5.22; Cl, 6.63; O, 9.02%.

RESULTS AND DISCUSSION

Lately, significant efforts have been made to broaden the scope of the synthesis of 1,8-dioxo-octahydroxanthene derivatives by catalytic condensation of dimedone and different aldehydes under suitable conditions like, solvent free, and using available, effective, recyclable, easily prepared nanoparticle catalyst. Nanoparticles often clump together due to their high surface energies, leading to larger particles with less surface area. Consequently, fewer surface-active sites became available in the catalyst. Stabilizing agents including surfactants or polymers are often employed to prevent nanoparticles from aggregating, while also potentially serving as functionalizing agents. Surface-modifying processes also lead to alterations in the electronic structure of the nanoparticle, which in turn impacts their catalytic activity. At present, conventional heterogeneous catalysts are being increasingly replaced by nanoparticles [34]. Smaller nanoparticles have larger surface areas and more exposed active sites. Nanoparticles possess greater contact surfaces with reactants, resulting in higher catalytic activity compared to traditional heterogeneous catalysts.

In this research we will discuss ZnO-NPs as one of the most important nanoparticle catalysts. Our research team synthesized ZnO-NPs by green way. An organic emulsifier with a polar moiety, such as a hydroxyl group, is necessary for the synthesis of ZnO at nanoparticle size, as shown in the present work. Additionally, propylene glycol, aloe vera, jojoba, caprylic, and flaxseed gel are ingredients we incorporate without using a stabilizer or emulsifier. In the supersaturated solution, the levels of Zn^{2+} and hydroxide ions rise, leading to the formation of larger and more heterogeneous ZnO particles through aggregation. The amount of stabilizer is critical for nanoparticle size, particularly with a high NaOH concentration. A higher concentration of stabilizer is required to achieve nanoparticles of the appropriate size, as a lower concentration produces larger nanoparticles. The ZnO-NPs were analyzed using TEM, XRD, and FTIR spectrophotometry.

Characterization for zinc oxide NPs

FTIR spectrophotometry (Figure 1) was utilized to analyze zinc oxide nanoparticles (ZnO-NPs) in various samples emulsified with different substances. The goal was to investigate the interaction between ZnO-NPs and the emulsifiers. Propylene glycol (a): FTIR analysis showed characteristic peaks associated with the C-H stretching, C-O stretching, and O-H bending vibrations of propylene glycol. These peaks provided insights into the interaction between

propylene glycol and the ZnO-NPs. Aloe Vera (b): The spectra for aloe vera exhibited peaks related to hydroxyl groups (O-H stretching), C-H stretching, and C=O stretching, reflecting its polysaccharide and flavonoid content. The interaction between aloe vera and ZnO-NPs was also analyzed. Jojoba (c): Jojoba oil's FTIR spectra showed typical peaks for wax esters, including C-H stretching, ester linkages (C=O), and lipophilic characteristics. The study focused on how jojoba oil modified or stabilized the ZnO-NPs. Caprylic Acid (d): Caprylic acid's FTIR spectra revealed peaks associated with carboxyl groups (C=O stretching), O-H bending, and C-H stretching, providing insights into how it interacted with the ZnO-NPs. Flaxseed Gel (e): Flaxseed gel exhibited peaks related to O-H stretching, C-H bending, and C=O stretching, corresponding to its polysaccharide and lipid content. The FTIR data helped understand how flaxseed gel interacted with the ZnO-NPs. The FTIR spectra helped to determine functional group interactions, surface modifications, and the overall stability of the ZnO-NPs in the presence of these emulsifiers. Each emulsifier influenced the nanoparticles in different ways, as reflected in the shifts or appearance of specific peaks in the spectra.

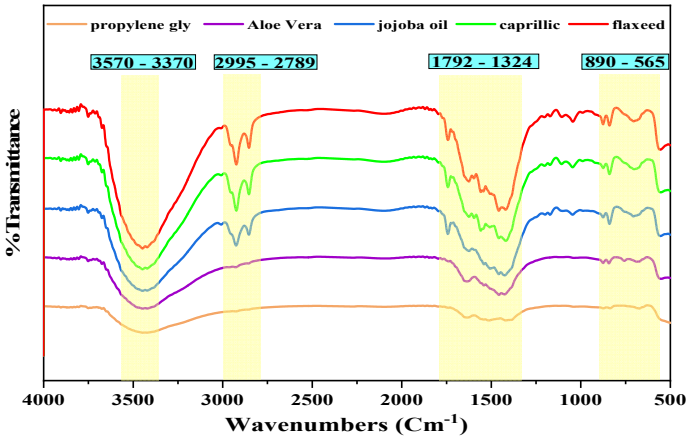

Figure 1. FTIR for analyze the interaction between ZnO-NPs and various emulsifiers. Each sample was represented by a different color.

In recent times, modern techniques like transmission electron microscopy (TEM), which uses transmitted electrons to create images, can assist in recognizing and visualizing tiny particles of various materials through high-definition images. Micrographs from the TEM/SAED analysis of ZnO-NPs produced using environmentally friendly techniques in a variety of natural emulsifiers demonstrate the formation of crystalline structures such as flags and roads (Figure 2). Depending on the kind of emulsifier used, the nanoparticle sizes change. The size of the nanoparticle falls within the range of 20-40 nm.

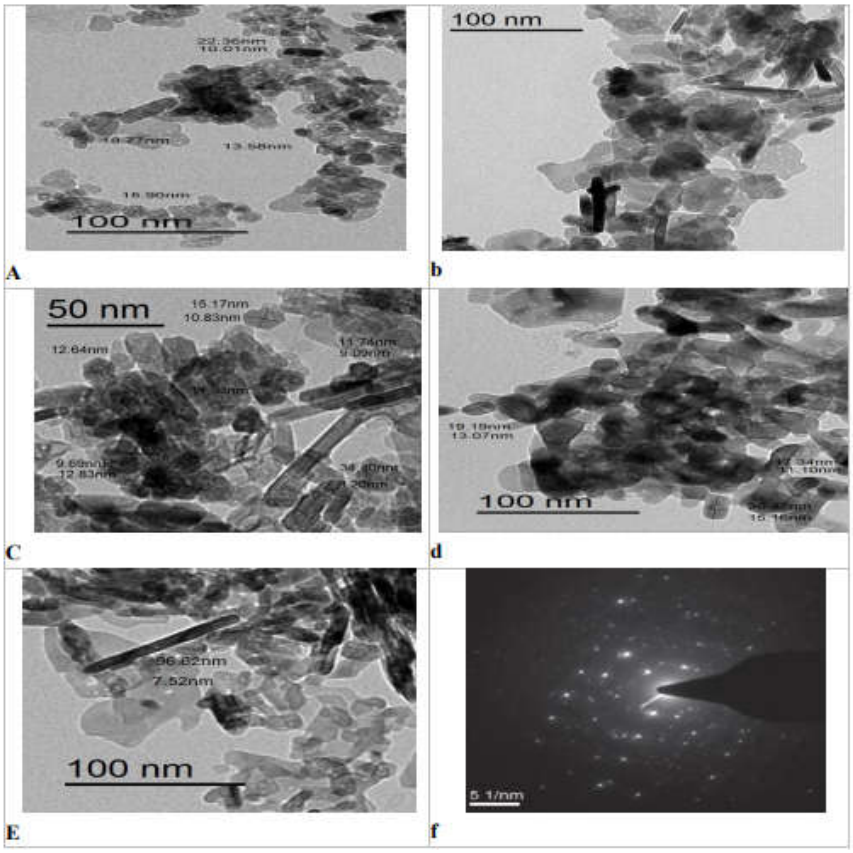

Figure 2. The transmission electron microscopy (TEM) of ZnO-NPs prepared using different emulsifiers. The figure includes several images and data points for various emulsifiers such as: (a) Aloe vera, (b) propylene glycol, (c) caprylic, (d) Jojoba, (e) flaxseed gel and (f) SAED pattern (selected area electron diffraction).

Frontier molecular orbitals (FMOs)

FMOs calculations were presented as an application that reflects many significant aspects about the distribution of electrons in the prepared compounds. The gap energy of xanthenes is important because it influences their electronic, optical, and chemical behavior, which in turn affects their applications in various fields like material science, chemistry, and electronics. Understanding and calculating this energy gap can help in designing better materials for a wide range of technologies, from sensors to advanced organic electronic devices. The LUMO orbitals were highly distribution on xanthene moiety with no distribution on others. Compound **9** HOMO plots π-orbitals were highly distributed on xanthene, sulfonate, and phenyl groups except for methyl group but the opposite for LUMO. Compound **10** shows the highest π-orbitals contribution on phenyl, Cl, and pyrazole ring with no other contribution. While, it's LUMO-orbitals show a high contribution on xanthene moiety but no other contribution. The above findings were illustrated in the E_{HOMO} and E_{LUMO} values, in Table 1. The E_{HOMO} values, which varied from 5.65 to 6.48 eV, were close

to each other, but E_{LUMO} values ranged from 1.59 to 2.40 eV. In which 5-nitro furfural derivative **6** shows (Figure 3) the highest E_{HOMO} and the lowest E_{LUMO}. The values of the HOMO–LUMO energy gap ($\Delta E_{H\text{-}L}$) ranged between 3.48 to 4.38 eV.

Table 1. The obtained theoretical HOMO energy (E_{HOMO}), LUMO energy (E_{LUMO}), HOMO–LUMO energy gap (ΔEH-L) in eV.

Molecules	E_{HOMO}	E_{LUMO}	$\Delta E_{H\text{-}L}$
1	-5.98	-1.61	4.37
2	-6.04	-1.62	4.42
3	-5.71	-1.59	4.11
4	-6.18	-1.79	4.38
5	-6.08	-1.76	4.31
6	-6.48	-2.40	4.07
7	-5.88	-1.66	4.22
8	-5.85	-1.65	4.20
9	-6.35	-1.97	4.38
10	-5.65	-1.81	3.84

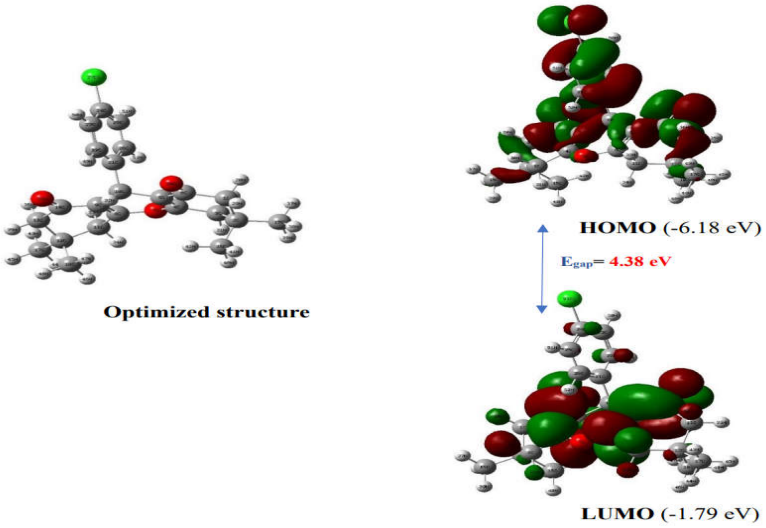

Figure 3. Optimized structure, HOMO and LUMO distribution patterns of xanthene derivative **6**.

Organic reaction

The xanthene derivatives were successfully synthesized by utilizing the ZnO-NPs as an efficient catalyst. The optimization of the reaction step occurred before the reaction, as outlined in Table 2. The resulting data showed that the ideal condition for this work involves utilizing a small amount of the ZnO-NPs in the reaction mixture of different aromatic aldehydes, dimedone, with stirring at 60-70 °C without the need for a solvent, and at the specific duration (Table 3, Scheme **1**). Xanthene derivatives (**1-10**) were synthesized, purified, and identified using various spectroscopic techniques (as detailed in the experimental section). The information presented in Table 3 indicates that the type of substituent in aldehydic rings impacts mainly in the reaction

time. The electron-releasing groups such as methyl group required a longer time compared with the electron withdrawing groups Cl, Br, NO_2 and sulfonate in the aldehydic ring.

Table 2. Optimization reaction among *p*-chlorobenzaldehyde (1 mol), and dimedone (2 mol) model example.

Entry	Catalyst	Time (min)	Solvent	Temp. °C	Yield %
1	Sm_2O_3/SiO_2 (20 mol %)	90	Free	60-70	60
2	ChCl-Ox (1:2) (0.5 mL)	15	ChCl-Ox	60	92
3	NH_4Cl (20 mol%)	120	Free	120	84
4	Ascorbic acid (15 mol %)	20	Free	70	86
5	ZnO (25 mol %)	60	Free	60-70	83
6	ZnO NPs (25 mol %)	20	Free	60-70	98
7	none	120	Free	60	Trace

Table 3. The reaction of 1 mol aromatic aldehydes and 2 mol dimedone (5,5-dimethyl-1,3-cyclohexanedione) to yield 1,8-dioxo-octahydroxanthene derivatives.

Comp.	Aromatic aldehydes	Yields%	Time (min)	M.P. (°C) Found	[Ref.]
1	4-Methylbenzaldehyde	90	150	170 -175	[35]
2	3-Methylbenzaldehyde	88	120	175-185	[36]
3	3-Methoxybenzaldehyde	95	90	164- 170	[37]
4	4-Chlorobenzaldehyde	98	20	220- 225	[37]
5	4-Bromobenzaldehyde	98	40	230-235	[37]
6	5-Nitrofuran-2-carbaldehyde	90	40	150-155	[38]
7	4-Formylphenyl benzoate	95	30	185-190	
8	4-Formylphenyl 4-methylbenzoate	93	60	175-180	
9	4-Formylphenyl 4-methylbenzene sulfonate	98	20	160-170	
10	3-(4-Chlorophenyl)-1-phenyl-1H-pyrazole-4-carbaldehyde	98	30	194-200	

The general reaction equation and the proposed method for the catalytic production of octahydroxanthenediones highlight the catalyst's pivotal role in activating the carbonyl carbon of an aldehyde, initiating the process. The procedure involves the placement of a pair of carbonyl oxygen electrons into the catalyst's vacant orbital, enabling benzaldehyde to function as an electron donor and facilitating the reaction. Initially, dimedone, which exists in a ketone-enol equilibrium due to the presence of an acidic hydrogen, undergoes a Knoevenagel condensation reaction with benzaldehyde, forming an intermediate (**1**). Subsequently, dimedone's proton, positioned favorably relative to $^{+}OH_2$ benzaldehyde, promotes water removal and aids in aldol formation. The addition of a second dimedone molecule results in the formation of an intermediate (**2**) through a Michael addition reaction. The mechanism promotes xanthene formation. The reaction was investigated to explain the potential of this catalytic process in yielding high amounts of octahydroxanthenediones. Refer to Table 3, and Scheme 1 for an overview of the structures, melting points, yields, and reaction times of compounds (**1-10**). Also, one of the routine steps in this type of reaction is measuring the recyclability degree of the catalyst and its efficiency. Therefore, the catalyst was filtered, dried, and reused, and no change occurred in its efficiency, even after this was repeated three times.

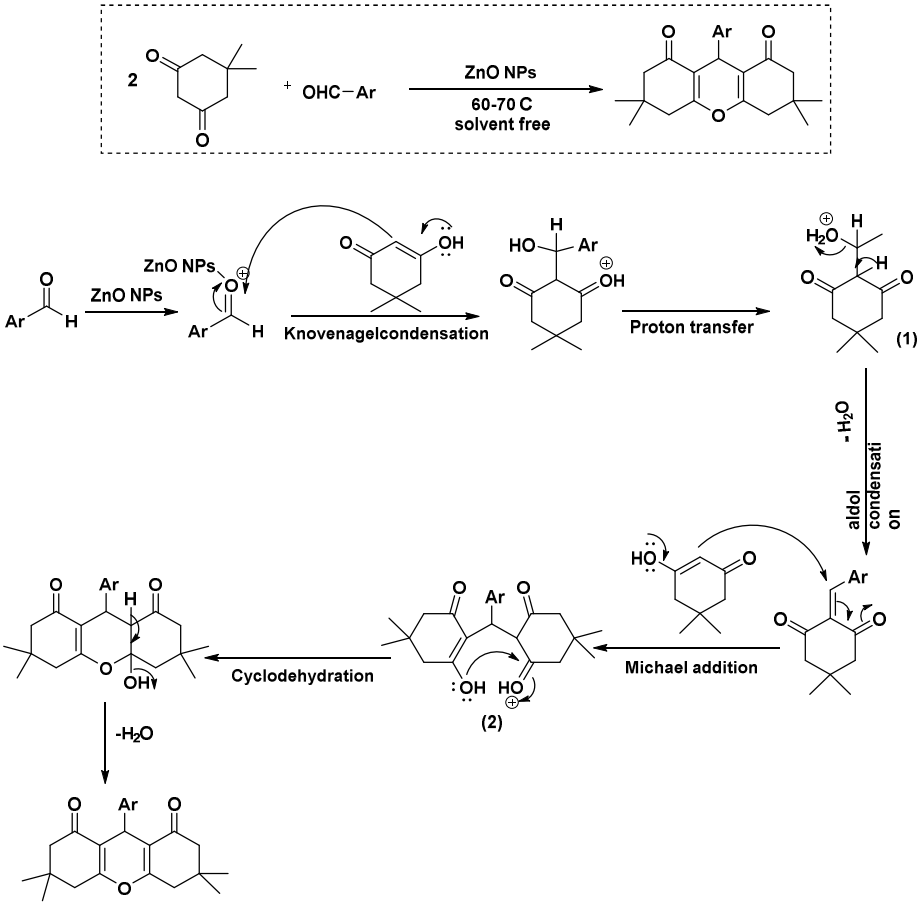

Scheme 1. The proposed reaction mechanism.

Biological activity and molecular docking

Drug discovery and development require very complicated steps, and in recent years, many scientific groups have used modern computer technologies to facilitate these steps and save time and money. Molecular docking software technologies help many scientific groups to achieve their research in drug discovery and development fields [39-43] the 3D structure of the targeted enzymes downloaded from the PDB website (enzymes ID code: 6y3c, 5kir and 3v99 for COX-1, COX-2 and 5-LOX respectively) and the software is MOE2015. Inflammation control is considered a big challenge related to the interference of many factors and enzymes. The COX-1, COX-2 and 5-LOX enzymes are catalysts in the formation of prostaglandins and leukotrienes which are endogenous factors that cause inflammation and pain.

Many COX-1 and COX-2 inhibitors (NSAIDs), such as ibuprofen, zileuton, indomethacin, and others, are very effective and widely used today. However, they all have the same side effects, such as peptic ulcers, hemorrhage, hypertension, kidney damage, and asthma, so all research groups are trying to develop this type of medication. The work that has been presented is regarded

as an initial investigation into the development of a novel anti-inflammatory medication with lower side effects. The presented study started by docking evaluation using MOE software and reference molecules indomethacin and zileuton. The data obtained in Table 4 showed the energy score calculation in kcal/mol that represents information about the binding strength between the prepared ligands and targeted enzymes COX-1, COX-2 and 5-LOX. Most of the prepared ligands give promising low energy values compared with reference molecules especially against COX-2 and 5-LOX more than COX-1. The less effective values towards COX-1 were explained by the conformation of the active site and steric hindrance for the prepared ligands.

Table 4. The energy scores values for binding between ligands and COX-1, COX-2 and 5-LOX.

Ligand	E-score kcal/mol (COX-1)	E-score kcal/mol (COX-2)	E-score kcal/mol (5-LOX)
L1	-6.27	-7.64	-7.30
L2	-6.51	-7.45	-7.31
L3	-6.48	-7.49	-7.02
L4	-5.58	-7.60	-6.67
L5	-6.37	-7.59	-7.57
L6	-6.49	-7.24	-7.42
L7	-6.63	-5.78	-7.74
L8	-6.63	-6.07	-8.69
L9	-7.04	-6.90	-8.08
L10	-6.60	8.05	-7.87
Zileuton	-5.52	-5.94	-5.79
Indomethacin	-6.35	-6.15	-7.012

From the two-dimensional photos (Figure 4) we can discover the amino acid residues at active side in COX-1, COX-2 and 5-LOX enzymes binding with **L6**. As a model example for three-dimensional diagrams, the interaction between **L6** and COX-2 showed that the main binding residues are ARG 513 and SER 353. The distance between nitro in **L6** and ARG 513 is explained in (2.21 Å).

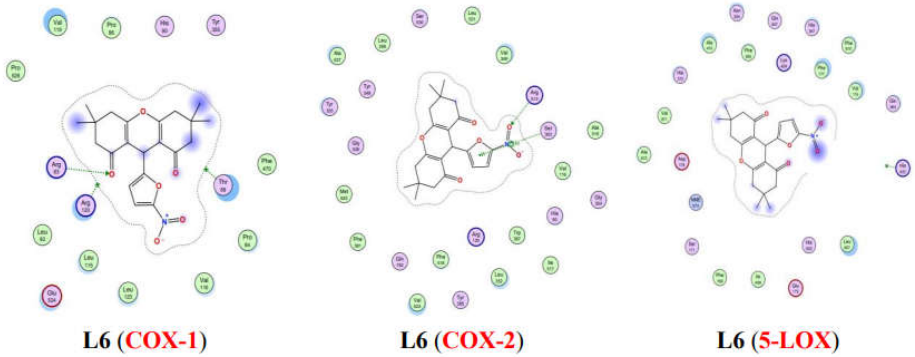

Figure 4. The binding active site in (COX-1 and COX-2).

Anti-inflammatory activity

Cyclooxygenase (COX) and lipoxygenase (LOX) are essential enzymes necessary for the conversion of arachidonic acid to eicosanoids, which play a crucial role in initiating

immunological responses, causing inflammation, and resolving inflammation [44]. COX has two isoenzymes, COX-1 and COX-2, which differ in many aspects and are responsible for the production of prostaglandins that play an important role in inflammation [45]. COX-1, COX-2, and 5-LOX are key pro-inflammatory enzymes involved in arachidonic acid metabolism [46]. While COX enzymes lead to the production of prostaglandins, 5-LOX catalyzes the formation of leukotriene B4, a mediator of inflammation and related diseases. Inhibiting 5-LOX can reduce leukotriene levels, potentially lowering the risk of cardiovascular and gastrointestinal issues [47].

The data depicted in Table 5 show the inhibitory effect of all the synthetic compounds on the activities of COX-1, COX-2, and 5-LOX enzymes. The derivative (**6**) showed the highest inhibitory effect on the activities of these enzymes at an equal concentration (1000 µg/mL) compared to the other tested compounds. It was noticed that (**6**) inhibited the activities of COX-1 and COX-2 by 77.28±0.18 and 79.53±0.18%, respectively, followed by the derivatives (**4**) (58.28±0.10 and 60.53±0.10%, respectively), (**4**) (58.36±0.10 and 60.61±0.10%, respectively), and (**10**) (58.45±0.10 and 60.70±0.10%, respectively). The derivatives (**2**) (49.55±0.05 and 51.80±0.05%, respectively) and (**1**) (49.61±0.03 and 51.86±0.03%, respectively) showed lower inhibitory effects compared to the standard indomethacin (a nonsteroidal anti-inflammatory drug), which inhibited the activities of COX-1 and COX-2 by 85.20±0.01 and 87.35±0.01%, respectively, at the same concentrations. Regarding the activity of the 5-LOX enzyme, it was found that (**6**) inhibited the activity of this enzyme by 64.38±0.18%, followed by the derivatives (**4**) (45.38±0.10%), (**7**) (45.4±0.10%), and (**10**) (45.55±0.10%). The derivatives (**2**) (36.65±0.05%) and **(1)** (36.71±0.03%) also showed lower inhibitory effects compared to the standard Zileuton, which inhibited the activity of this enzyme by 72.20±0.01%. The other synthetic derivatives (**4**, **6**, **7**, and **10**) showed the lowest inhibitory effect on the activities of COX-1, COX-2, and 5-LOX enzymes. Regarding the IC_{50} values, a low IC_{50} indicates a higher inhibition percentage against the activities of COX-1, COX-2, and 5-LOX enzymes and hence higher anti-inflammatory activity. Therefore, the lowest IC_{50} values against COX-1, COX-2 and 5-LOX enzymes were found with the compounds (**6**) (5.96±0.04, 5.27±0.02 and 7.77±0.03 mg/mL, respectively), followed by the derivatives (**4**) (7.90±0.07, 6.92±0.02 and 11.02±0.05 mg/mL, respectively), (**7**) (7.89±0.07, 6.91±0.02 and 11.00±0.05 mg/mL, respectively), and (**10**) (7.88±0.07, 6.90±0.02 and 10.98±0.05 mg/mL, respectively) compared to the corresponding standards (5.41±0.04, 4.80±0.01 and 6.93±0.02 mg/mL, respectively) which showed a lower IC_{50} value. The derivatives (**2**) (9.30±0.07, 8.09±0.02 and 13.64±0.05 mg/mL, respectively) and (**1**) (9.28±0.06, 8.08±0.02 and 13.62±0.03 mg/mL, respectively) showed higher IC_{50} values.

Table 5. *In vitro* anti-inflammatory activity at equal concentrations (1000 µg/mL) and the median inhibitory concentrations (IC_{50}) of different synthetic derivatives against the activities of COX-1, COX-2 and 5-LOX enzymes.

	COX-1		COX-2		5-LOX	
	Inhibition (%)	IC_{50} (µg/mL)	Inhibition (%)	IC_{50} (µg/mL)	Inhibition (%)	IC_{50} (µg/mL)
1	49.61 ± 0.03	9.28 ± 0.06	51.86 ± 0.03	8.08 ± 0.02	36.71 ± 0.03	13.62 ± 0.03
2	49.55 ± 0.05	9.30 ± 0.07	51.80 ± 0.05	8.09 ± 0.02	36.65 ± 0.05	13.64 ± 0.05
3	38.90 ± 0.05	11.84 ± 0.10	41.15 ± 0.05	10.18 ± 0.03	26.00 ± 0.05	19.23 ± 0.08
4	58.28 ± 0.10	7.90 ± 0.07	60.53 ± 0.10	6.92 ± 0.02	45.38 ± 0.10	11.02 ± 0.05
5	38.96 ± 0.03	11.82 ± 0.08	41.21 ± 0.03	10.17 ± 0.03	26.06 ± 0.03	19.19 ± 0.05
6	77.28 ± 0.18	5.96 ± 0.04	79.53 ± 0.18	5.27 ± 0.02	64.38 ± 0.18	7.77 ± 0.03
7	58.36 ± 0.10	7.89 ± 0.07	60.61 ± 0.10	6.91 ± 0.02	45.46 ± 0.10	11.00 ± 0.05
8	38.78 ± 0.06	11.88 ± 0.08	41.03 ± 0.06	10.21 ± 0.01	25.88 ± 0.06	19.33 ± 0.03
9	38.82 ± 0.06	11.86 ± 0.08	41.07 ± 0.06	10.20 ± 0.01	25.92 ± 0.06	19.29 ± 0.03
10	58.45 ± 0.10	7.88 ± 0.07	60.70 ± 0.10	6.90 ± 0.02	45.55 ± 0.10	10.98 ± 0.05
STD	Indomethacin				Zileuton	
	85.20 ± 0.01	5.41 ± 0.04	87.35 ± 0.01	4.80 ± 0.01	72.20 ± 0.01	6.93 ± 0.02

Values were calculated from three replicates and expressed as mean ± SE.

The active site of cyclooxygenase (COX) consists of a long hydrophobic channel with a narrow entrance. While the active sites of COX-1 and COX-2 are similar, COX-2 features a larger binding cavity, enabling the development of selective inhibitors. Additionally, COX-2 has a side pocket above the entrance of its binding site [48]. The synthetic compounds inhibited COX enzyme activity by binding to the hydrophobic region of the COX-2 binding site, rather than the side pocket region. This selective inhibition may be due to differences in the chemical structure between indomethacin and the derivatives. Additionally, these compounds likely selectively target COX-2 through hydrogen bond interactions with key amino acids in the enzyme's catalytic domain. The binding was further stabilized by hydrophobic interactions in both the hydrophobic and lobby regions of the COX binding site [49]. For 5-LOX inhibition, the inhibitory effect of these synthetic compounds might be contributed by a hydrogen bond interaction with the amino acid residue in the active site of the enzyme. They inhibited the activity of this enzyme by similar mechanism by which Zileuton interact with the active site of the enzyme. On the other hand, hydrophobic and polar interactions were the main contributors to the activity of these compounds with the amino acid residues in the binding interactions of 5-LOX [50].

CONCLUSION

Zinc oxide was successfully prepared using natural oils such as jojoba oil, aloe vera, propylene glycol, flaxseed gel, and caprylic acid as emulsifying and stabilizing agents to prepare nano zinc oxide in an eco-friendly manner. Techniques such as FTIR (fluorochromic infrared spectroscopy), XRD (X-ray diffraction), and TEM (transmission electron microscopy) were used to elucidate the chemical composition of the prepared nanoparticles. ZnO-NPs was successfully used as a catalyst to prepare xanthine compounds through a one-step reaction, where two moles of diamidon and aromatic aldehyde were mixed under solvent-free conditions at 60-70 °C. After the reaction was completed in the specified time, the products were separated and their structural structures were confirmed using IR, NMR, and TEM. The data obtained from the DFT (density functional theory) calculations, docking and biological evaluation as inhibitors of COX1, COX2 and 5-LOX enzymes explained that there are four derivatives (**4**, **6**, 7, and **10**) can presented in vivo anti-inflammatory test.

Funding

This research was funded by King Saud University, Riyadh, Saudi Arabia, through the Ongoing Research Funding program - Research Chairs (ORF-RC-2025-0106).

ACKNOWLEDGMENTS

The authors are grateful to King Saud University, Riyadh, Saudi Arabia, for funding this work through the Ongoing Research Funding program - Research Chairs (ORF-RC-2025-0106).

REFERENCES

1. Rahman N.; Nongkhlaw, R. Recent advances in organo-nanocatalysis in the field of green organic synthesis. *Org. Chem.* **2018**, VI, 272-313.
2. Khodabakhshi, S.; Khaleghi Abbasabadi, M.; Heydarian, S.; Gharehzadeh Shirazi, S.; Marahel, F. Fe_3O_4 Nanoparticles as highly efficient and recyclable catalyst for the synthesis of 4-hydroxy-3-[aryloyl(benzamido)methyl]coumarin under solvent-free conditions. *Lett. Org. Chem.* **2015**, 12, 465-470.

3. Tajbakhsh, M.; Farhang, M., Baghbanian, S. M.; Hosseinzadeh, R.; Tajbakhsh, M. Nano magnetite supported metal ions as robust, efficient and recyclable catalysts for green synthesis of propargylamines and 1,4-disubstituted 1,2,3-triazoles in water. *New J. Chem.* **2015**, 39, 1827-1839.
4. Mohan, A.C.; Renjanadevi, B. Preparation of zinc oxide nanoparticles and its characterization using scanning electron microscopy (SEM) and X-ray diffraction (XRD). *Proc. Technol.* **2016**, 24, 761-766.
5. Salim**,** E. Influence of ethocel polymer (Ec) loaded with inorganic nanoparticles (ZnO-NPs) on the chemical and physical properties of wooden paper. *EJARS* **2024**, 14, 11-18**.**
6. Dey, S.; lochan Mohanty, D.; Divya, N.; Bakshi, V.; Mohanty, A.; Rath, D.; Das, S.; Mondal, A.; Roy, S.; Sabui, R. A critical review on zinc oxide nanoparticles: Synthesis, properties and biomedical applications. *Intelligent Pharmacy* **2025**, 3, 53-70.
7. Hazim, K.; Khudair, Z.F.; Kadhim, I.K.; Mohamed, L.; Hameed, G.F.; Alyasiri, F. J. Biosynthesis, antibacterial activity, the photocatalytic performance of ZnO NPs by use of leaf extract of the plant primo fiore. *Pakistan J. Med. Health Sci.* **2022**, 16, 456-459.
8. Zhu, L.; Li, Y.; Zeng, W. Hydrothermal synthesis of hierarchical flower-like ZnO nanostructure and its enhanced ethanol gas-sensing properties, *Appl. Surf. Sci.* **2018**, 427, 281-287.
9. Brahma**,** S.; Shivashankar, S.A. Microwave irradiation assisted rapid growth of ZnO nanorods over metal coated/electrically conducting substrate, *Mater. Lett.* **2020**, 264, 127370**.**
10. Khatab, T.K.; Abdelghany, A.M.; Soliman, H.A. V_2O_5/SiO_2 as a heterogeneous catalyst in the synthesis of bis (indolyl) methanes under solvent free condition. *Silicon* **2018**, 10, 703-708.
11. Khatab, T.K.; Kandil, E.M.; Elsefy, D.E.; El-Mekabaty, A. A one-pot multi-component catalytic synthesis of new 1H-pyrazole-1-carbothioamide deriva-tives with molecular docking studies as COX-2 inhibitors. *Biointerface Res. Appl. Chem*. **2021**, 11, 13779-13789.
12. Khatab, T.K.; Hassan, A.S. Computational molecular docking and in silico ADMET prediction studies of pyrazole derivatives as COVID-19 main protease (Mpro) and papain-like protease (PLpro) inhibitors. *Bull. Chem. Soc. Ethiop*. **2023**, 37, 449-461.
13. Soliman, H.A.; Khatab, T.K. New approach for tetrachlorosilane promoted one-pot, condensation reaction for tetrahydrobenzo [a] xanthene-11-ones with docking validation as aurora kinase inhibitor. *Silicon* **2018**, 10, 229-233.
14. Elmorsy S.S.; Badawy D.S.; Khatab, T.K. Chemoselective bromination in a two-step substitution under the influence of tetrachlorosilane and N-bromosuccinimide. *Phosphorus Sulfur Relat. Elem.* **2006**, 181, 2005-2012.
15. Khatab, T.K.; El-Mekabaty A.; Gamala, Z.M.; Kandil, E. An efficient catalytic synthesis of 1,8-dioxo-octahydroxanthene derivatives with anti-oxidant scanning. *Egypt. J. Chem.* **2018**, 61, 4, 661-666.
16. Abdel-Latif, E.; Khatab, T.K.; Fekri, A.; Khalifa, M.E. Synthesis of new binary thiazole-based heterocycles and their molecular docking study as COVID-19 main protease (Mpro) inhibitors. *Russ. J. Gen. Chem.* **2021**, 91, 1767-1773.
17. Chibale, K.; Visser, M.; Van Schalkwyk, D.; Smith, P.J.; Saravanamuthu, A.; Fairlamb, A. H. Exploring the potential of xanthene derivatives as trypanothione reductase inhibitors and chloroquine potentiating agents. *Tetrahedron* **2003**, 59, 2289-2296.
18. Ion, R.M.; Planner, A.; Wiktorowicz, K.; Frackowiak, D. The incorporation of various porphyrins into blood cells measured via flow cytometry, absorption and emission spectroscopy. *Acta Biochim. Pol.* **1998**, 45, 833-845.
19. Kalinski, C.; Lemoine, H.; Schmidt, J.; Burdack, C.; Kolb, J.; Umkehrer, M.; Ross, G. Multicomponent reactions as a powerful tool for generic drug synthesis. *Synth.* **2008**, 24, 4007-4011.

20. Limsuwan, S.; Trip, E.N.; Kouwen, T.R.H.M.; Piersma, S.; Hiranrat, A.; Mahabusarakam, W.; Voravuthikunchai, S.P.; Van Dijl, J.M.; Kayser, O. Rhodomyrtone: A new candidate as natural antibacterial drug from *Rhodomyrtus tomentosa*. *Phytomedicine* **2009**, 16, 645-651.
21. Bekaert, A.**;** Andrieux, J.**;** Plat, M. New total synthesis of bikaverin. *Tetrahedron Lett.* 1992, 33, 2805-2806.
22. Banerjee A.; Mukherjee, A.K. Chemical aspects of santalin as a histological stain. *Stain Technol.* **1981**, 56, 83-85.
23. Sarma, R.J.; Baruah, J.B. One step synthesis of dibenzoxanthenes. *Dyes Pigm.* **2005**, 64, 91-92,
24. Quintás, D.; García, A.; Domínguez, D. Synthesis of spiro[pyrrolidine or piperidine-3,9′-xanthenes] by anionic cycloacylation of carbamates. *Tetrahedron Lett.* **2003**, 44, 9291-9294**.**
25. Knight, D.W.; Little, P.B. The first efficient method for the intramolecular trapping of benzynes by phenols: a new approach to xanthenes. *J. Chem. Soc. Perkin. Trans.* **2001**, 1, 1771-1777.
26. Bekaert, A.; Andrieux, J.; Plat, M. New total synthesis of bikaverin. *Tetrahedron Lett.* **1992**, 33, 2805-2806.
27. Kuo, C.W.; Fang, J.M. Synthesis of xanthenes, indanes, and tetrahydronaphthalenes via intramolecular phenyl–carbonyl coupling reactions. *Synth. Commun.* **2001**, 31, 877-892.
28. Casiraghi, G.; Casnati, G.; Cornia, M. Regiospecific reactions of phenol salts: Reaction-pathways of alkylphenoxy-magnesiumhalides with triethylorthoformate. *Tetrahedron Lett.* **1973**, 14, 679-682**.**
29. Seyyedhamzeh, M.**;** Mirzaei, P.**;** Bazgir**,** A. Solvent-free synthesis of aryl-14*H*-dibenzo[*a*,*j*]xanthenes and 1,8-dioxo-octahydro-xanthenes using silica sulfuric acid as catalyst. *Dyes. Pigm.* **2008**, 76, 836-839.
30. Wang, X.S.; Shi, D.Q.; Li, Y.L.; Chen, H.; Wei, X.Y.; Zong, Z.M. Clean synthesis of 1-oxo-hexahydroxanthene derivatives in aqueous media catalyzed by TEBA. *Synth. Commun.* **2005**, 35, 97-104.
31. Das, B.; Thirupathi, P.; Mahender, I.; Reddy, V.S.; Rao, Y.K. Amberlyst-15: An efficient reusable heterogeneous catalyst for the synthesis of 1,8-dioxo-octahydroxanthenes and 1,8-dioxo-decahydroacridines, *J. Mol. Catal. A Chem.* **2006**, 247, 233-239**.**
32. Das, B.; Thirupathi, P.; Reddy, K.R.; Ravikanth, B.; Nagarapu, L. An efficient synthesis of 1,8-dioxo-octahydroxanthenes using heterogeneous catalysts. *Catal. Commun.* **2007**, 8, 535-538.
33. Ozin, G.A.; Arsenault, A.C.; Cademartiri, L. Nanochemistry: A chemical approach to nanomaterials. *RCS* **2009**, 876, https://doi.org/10.1039/9781849737395.
34. Sangeetha, C.C.; Madivanane, R.; Pouchaname, V. The vibrational spectroscopic (FT-IR and FT Raman, NMR, UV) study and HOMO and LUMO analysis of phthalazine by DFT and HF studies. *IJERGS* **2014**, 2, 222-251.
35. Shirini, F.; Yahyazadeh, A.; Mohammadi K. One-pot synthesis of various xanthene derivatives using ionic liquid 1,3-disulfonic acid imidazolium hydrogen sulfate as an efficient and reusable catalyst under solvent-free conditions. *Chinese Chem. Lett.* **2014**, 25, 341-347.
36. Heravi, M.M.; Alinejhad, H.; Bakhtiari, K.; Oskooie, H.A. Acid catalyzed solvent free synthesis of 10-aryl-7,7-dimethyl-6,7,8,10-tetrahydro-9H-[1,3]-dioxolo [4,5-b]xanthen-9-ones and 12-aryl-9,9-dimethyl-8,9,10,12-tetrahydro-11H-benzo[a]xanthen-11-one. *Mol. Divers.* **2010**, 14, 621-626.
37. Khoeiniha, R.; Ezabadi, A.; Olyaei, A. An efficient solvent-free synthesis of 1,8-dioxooctahydroxanthenes using $Fe_2(SO_4)_3.7H_2O$ as catalyst. *Chem. Commun.* **2016**, 4, 273-282.
38. Nikolaeva, T.G.; Shchekotikhin, Y.M.; Ponomarev, A.S.; Kriven'Ko, A.P. Peculiarities of formation of decahydroacridine-1,8-diones on the basis of 1,3-dioxocyclohexane compounds in various media. *Chem. Heterocycl. Compd.* **2000**, 36, 403-409.

39. Soliman, H.A.; Khatab, T.K.; Abdel-Megeid, F.M. Utilization of bromine azide to access vicinal-azidobromides from arylidene malononitrile. *Chinese Chem. Lett.* **2016**, 27, 1515-1518.
40. Said, G.E.; Tarek, M.; Al-Wasidi, A.S.; Naglah, A.M.; Almehizia, A.A.; Khatab, T.K. Niacin based MOF as efficient nano-catalyst in the synthesis of some new benzothiazoles and benzimidazoles as anti-Alzheimer (AChE inhibitors), *J. Mol. Struct.* **2024**, 1311, 138462.
41. Al-Wasidi, A.S.; AlMohisen, H.M.; Almehizia, A.A.; Naglah, A.M.; Tarek, M.; Said, G.E.; Khatab, T.K. Cu-Vit B3 MOF solvothermal preparation, characterization and evaluation as HIV-1 RNA replication inhibitor. *J. Mol. Struct.* **2024**, 1317, 139120.
42. lmehizia, A.A.; Naglah, A.M.; Zen, A.A.; Khatab, T.K.; Hassan, A.S. TCS/$ZnCl_2$ as a controlled reagent for the Michael addition and heterocyclic cyclization based on the phenyl pyrazolone scaffold with docking validation as a COVID-19 protease inhibitor. *Bull. Chem. Soc. Ethiop*. **2024**, 38, 1119-1127.
43. Shaker, N.; Kandil, E. M.; Osama, Y.; Khatab, T.K.; Khalifa, M.E. $ZnCl_2/SiO_2$ as a new catalyst for the eco-friendly synthesis of n- thiocarbamoyl pyrazoles and thiosemicarbazones with antioxidant and molecular docking evaluation as (UppS) inhibitor. *Curr. Org. Chem.* **2021**, 25, 2037-2044.
44. Boittier, E.D.; Tang, Y.Y.; Buckley, M.E.; Schuurs, Z.P.; Richard, D.J.; Gandhi, N.S. Assessing molecular docking tools to guide targeted drug discovery of CD38 inhibitors. *Int. J. Mol. Sci.* **2020**, 21, 1-19.
45. Bošković, J.; Dobričić, V.; Mihajlović, M.; Kotur-Stevuljević, J.; Čudina, O. Synthesis, evaluation of enzyme inhibition and redox properties of potential dual COX-2 and 5-LOX inhibitors. *Pharma.* **2023**, 16, 549.
46. Md Idris, M.H.; Mohd Amin, S.N.; Mohd Amin, S.N.; Nyokat, N.; Khong, H.Y.; Selvaraj, M.; Salleh, M.Z. Flavonoids as dual inhibitors of cyclooxygenase-2 (COX-2) and 5-lipoxygenase (5-LOX): molecular docking and in vitro studies. *J. Basic Appl. Sci.* **2022**, 11, 1-9.
47. Kaur, G.; Silakari O. Multiple target-centric strategy to tame inflammation. *Future Med. Chem.* **2017**, 9, 1361-1376.
48. Kutil, Z.; Temml, V.; Maghradze, D.; Pribylova, M.; Dvorakova, M.; Schuster, D.; Landa, P. Impact of wines and wine constituents on cyclooxygenase-1, cyclooxygenase-2, and 5-lipoxygenase catalytic activity. *Mediat. Inflamm.* **2014**, 1-8.
49. Mabrouk, A.A.; Tadros, M.I.; El-Refaie, W.M. Improving the efficacy of Cyclooxegenase-2 inhibitors in the management of oral cancer: Insights into the implementation of nanotechnology and mucoadhesion. *J. Drug Deliv. Sci. Technol.* **2021**, 61, 102240.
50. Rudrapal, M.; Eltayeb, W.A.; Rakshit, G.; El-Arabey, A.A.; Khan, J.; Aldosari, S.M.; Abdalla, M. Dual synergistic inhibition of COX and LOX by potential chemicals from Indian daily spices investigated through detailed computational studies. *Sci. Rep.* **2023**, 13, 8656.